Daniela FIEDLER, Bsc

Simulation of compaction behaviour of non-spherical particles with Multi Particle Finite Element Method

MASTER'S THESIS

to achieve the university degree of
Diplom-Ingenieur

Master's degree programme: Chemical and Process Engineering

submitted to
GRAZ UNIVERSITY OF TECHNOLOGY

Supervisor:
Univ.-Prof. Dipl.-Ing. Dr. Johannes KHINAST
INSTITUTE OF PROCESS AND PARTICLE ENGINEERING

Co-Supervisor:
Dipl.-Ing. Dipl.-Ing. Peter LOIDOLT, BSc
INSTITUTE OF PROCESS AND PARTICLE ENGINEERING

Graz, Mai 2018

AFFIDAVIT

I declare that I have authored this thesis independently, that I have not used other than the declared sources/resources, and that I have explicitly indicated all material which has been quoted either literally or by content from the sources used. The text document uploaded to TUGRAZonline is identical to the present master's thesis.

Date	Signature

Acknowledgement

First of all I would like to thank Peter Loidolt, who is for me the Zen in the Multi Particle Finite Element Method and as well in the stress space. He lend an ear whenever needed and gave helpful input and support. Thank You Peter for guiding me through my master thesis!

I would also like to thank Prof. Johannes Khinast for giving me the opportunity to work on this project and getting an insight in the world of research and pharmaceutical engineering.

Special thanks go to the whole research team , Andreas B. & Andreas K. & Stefan M., for turning every day in the office in a good day, needless to say with or without coffee.

Last but not least I want to thank Simon and my family for all their precious support throughout my whole studies. Thank You!

Abstract

The Multi Particle Finite Element Method gains importance in the field of particle simulation. Combining Discrete Element Method and Finite Element Method enables depicting and analysing the compaction process and understanding powder behaviour. The compaction process of tablets is a crucial unit operation in the pharmaceutical manufacturing path. Commencing from an available code to simulate the compression behaviour of spheres including cohesive contacts, non-spherical particles are implemented to mimic fibrous microcrystalline cellulose. After studying the convergence behaviour of the simulation parameters different particle rotations and the effects on the strength after compression are examined. During these convergence studies a mesh fineness of four elements per particle diameter, a particle number of 100 particles in the RVE, a solver time step size of 10^{-4} s and a mass scaling of 10^4 are found as optimal. For non-spherical particles the strengths show different behaviours regarding the yield test direction. One revolution per particle length leads to the maximum strengths observed, whereas minimum strengths are obtained for zero and a half revolution per particle length. The proposed simulation code allows for mechanistic understanding of the particle behaviour and thus for examining influences on the strengths, such as equivalent pressure after compression equivalent and elastic strain during unloading.

Kurzfassung

Die Multipartikel-Finite-Elemente-Methode gewinnt im Bereich der Partikelsimulation an Relevanz. Die Kombination von Diskrete-Element-Methode und Finite-Elemente-Methode ermöglicht die Darstellung und Analyse des Verdichtungsprozesses und verbessert das Verständnis des Pulververhaltens. Der Verdichtungsprozess von Tabletten ist ein zentraler Prozessschritt in der pharmazeutischen Produktion. Ausgehend von einem verfügbaren Code zur Simulation des Kompressionsverhaltens von Kugeln einschließlich kohäsiver Kontakte, werden nicht-sphärische Partikel zur Modellierung von faseriger mikrokristalliner Cellulose implementiert. Nach der Untersuchung des Konvergenzverhaltens der Simulationsparameter werden verschiedene Rotationsgrade und die Auswirkungen auf die Festigkeit nach der Kompression analysiert. Die Konvergenzstudien zeigen optimale Balance zwischen Genauigkeit und Effizienz bei einer Netzfeinheit von vier Elementen pro Partikeldurchmesser, eine Partikelanzahl von 100 Partikeln im RVE, eine Solverzeitschrittweite von 10^{-4} s und einem Massenskalierungsfaktor von 10^4. Bei nichtsphärischen Partikeln zeigen die Festigkeiten ein unterschiedliches Verhalten abbhängig von der Testrichtung. Maximale Festigkeiten werden bei einer Umdrehung pro Partikellänge beobachtet, während bei null und halber Umdrehung pro Partikellänge minimale Festigkeiten erreicht werden. Der vorgeschlagene Simulationscode ermöglicht ein mechanistisches Verständnis des Partikelverhaltens und damit die Untersuchung von verschiedenen Einflüssen auf die Festigkeiten, wie z.B. äquivalentem Druck nach der Kompaktierung und äquivalenter elastischer Dehnung bei der Entlastung.

Contents

Chapter 1

Introduction

During pharmaceutical manufacturing one has to deal inevitable with powders. Unit operations are devoted to create particles, modify those and form the desired product. Crystallisation, milling, blending, granulation and the final processing to the desired drug delivery form are just a few unit operations in the pharmaceutical manufacturing path. Muzzio et al. [18] describe the pharmaceutical manufacturing path and emphasised the importance of powder and particle technology in the pharmaceutical industry.
As the behaviour of powders not only depends on material properties but also on environmental parameters, such as temperature, humidity and the history of the powder, it is obvious that a deep understanding and wide knowledge of material properties and behaviour of powders is crucial. To give an example, Sinka et al. [22] focused on the filling and compaction of the tableting process and examined important process parameters and its influences on the final material properties of the tablets and stated the complexity of the tablet compression process.

To place importance on the mechanical material properties they are mentioned in this part. The Young's Modulus E is a measure of stiffness and describes the reversible elastic deformation reaction of the powder to external stress. If the elastic limit is reached irreversible plastic deformation occurs. A measure to describe the plasticity of a material is the yield strength, which is critical for the tablet design. The tensile strength equals the maximum strength to be withstand by the material with tensile load before material breakage. Another measure is the hardness of a material which is commonly measured by indentation and characterises the resistance of a solid material to irreversible deformation. Sun et al. [25] examined mechanical material properties of pharmaceutical solids, set them into correlation and concluded the effects on the tableting process.
Furthermore, powder behaviour is strongly effected by particle-particle interaction and the resulting inter-particle forces. For powders these inter particle forces might be dominated by cohesion which may arise from electrostatic, capillary and/or Van der Waals forces. Understanding cohesion and mechanical material properties is essential for setting up a mechanistic model to emulate powder behaviour.

Two methods for powder flow simulation gained importance in the recent years: the *Discrete Element Method* (DEM) and the *Finite Element Method* (FEM). In DEM powders are modelled as an assembly of particles. Most times each particle is modelled as a sphere because of simplification reasons. Since the particles are rigid no deformation is considered. Overlapping of particles is interpreted as contact and leads to contact forces. To gain information about the system, the equations of motion are solved for every particle. The advantage of DEM in particle flow simulations is the resolution of every particle in the powder. Recent studies with DEM on powder compaction include Persson et al. [19] and Jerier et al. [15]. In comparison, the FEM models the powder as a continuum. Which is the reason that single particles can not be tracked and analysed anymore. However the simulation becomes more efficient in terms of simulation time as the property of each particle does not need to be calculated every time step. The FEM approach bases on a material model, which in contrast to DEM, is difficult to determine. The compaction process of a pharmaceutical powder was analysed with FEM in the work of Wu et al. [26]. Combining these two methods introduces the *Multi Particle Finite Element Model* (MPFEM). MPFEM modelling, in detail described in [27], treats every single particle as own entity with its individual mesh. The particle deformation is modelled and depends on the material properties of the particles and loading conditions. Loading conditions include body, external and contact forces. With the MPFEM approach the material model for FEM simulations can be determined, information about the tensile and compression strengths can be obtained and the simulation might be more accurate than with DEM simulations. However, MPFEM is more expensive.

Currently the pharmaceutical industry takes an overall turn from trial and error practices to quality by design. Loidolt et al. [17] contributed to this development and evolved a simulation environment in *Abaqus CAE - Simulia*™ with the goal to determine material models of powders based on MPFEM. A novel kind of boundary conditions was introduced to circumvent the influence of boundary effects. The simulation environment was designed in such a way to enable arbitrary variation of simulation and material parameters and to ease the convergence study process. However they used in their work a spherical particle shape. As powder particles in reality rarely have the form of spheres and the simulation environment of Loidolt et al. [17] allows for implementing different shapes and size the subject of this thesis arose.
This master thesis' intention is the introduction of non-spherical particles in the simulation procedure, conduct convergence studies to verify the used model parameters and investigate the effects of different geometrical particle shapes on resulting tension, compaction and isostatic yield strengths after uni-axial compaction. Following chapters are focusing on the basic structure, important key points and introduced changes to the work

of Loidolt et al. [17].

Chapter 2

Methods & Material

2.1 Material

Microcrystalline cellulose (MCC) is an important material in the pharmaceutical industry, mainly used as a binding and filling material in the production of pharmaceutical tablets. Since MCC not only enhances the binding properties but also the compaction behaviour, numerous works study the compaction and deformation behaviour (Edge et al. [3], Eichhorn et al. [4], Hancock et al. [9], Sun [24]). Depending on the process parameters and the production path of the MCC the size, shape and particle distribution vary. MCC may occur in a particulate or fibrous shape.

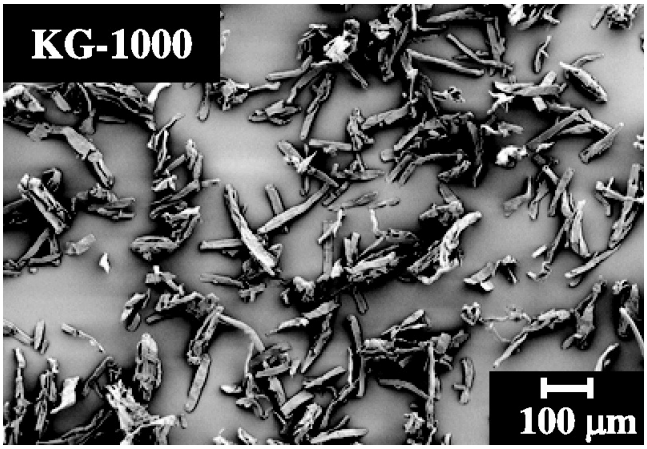

Figure 2.1: Scanning electron microscope picture of MCC particles (from Horio et al. [12]). Particles are poly-disperse distributed, slighlty twisted and in fibrous shape.

Zhao et al. [30] measured the size and shape of untreated cotton linters. The macrofibrils length varies between 300-500 µm and the diameter between 10-20 µm. Gaudreault et al. [6] determined the average particle size of 24 µm of a MCC powder by light scattering. The cellulose fibres are poly-disperse distributed and slightly twisted (Figure 2.1). The size and shape of the implemented particles in the simulation base on these measures.

The particles are modelled as elongated helical spring. Due to efficiency and practicability issues the particle distribution in the simulation is mono-disperse and the length to diameter ratio is about one decimal power smaller. The size measures of the particles are chosen four decimal powers bigger. Because of a quasi-static simulation (no inertial effects occur) the compression strength results are not influenced.

Table 2.1: Diameter, length, revolution and offset of the particles used to mimic cellulose fibres.

Particle No.	Length [m]	Diameter [m]	Offset [m]	Revolution
P0	0.3	0.15	0.04	0.0
P1	0.3	0.15	0.04	0.25
P2	0.3	0.15	0.04	0.5
P3	0.3	0.15	0.04	0.75
P4	0.3	0.15	0.04	1.0

Different forms of particles are studied (Table 2.1). The diameter, length and offset of the helical spring are kept constant and the effect of different revolutions per particle length on the compression strengths is examined. The offset defines the distance between the center of the fibre and the rotational axis. In Equation (2.1) the mathematical description of the revolution is shown and can be expressed as the number of revolutions per particle length.

$$revolution = \frac{no.\ revolutions}{particle\ length} \tag{2.1}$$

2.2 Methods

Overall goal is to set up a micromechanical model to determine macroscopic material properties of powders, e.g. Young's Modulus and uni-axial yield strengths. This macroscopic material properties can later be used in FEM simulations. Following procedure is performed to pave the way to a micromechanical model of powders: With the open-source DEM software *LIGGGHTS®* [16] a random particle packing is generated. This packing's aim is to depict a Representative Volume Element (RVE) of the powder. Afterwards the packing is transferred into the simulation environment of *Abaqus CAE - Simulia™* to perform the MPFEM simulations.

2.2.1 Representative Volume Element (RVE)

To emphasise the importance of the RVE a short overview is given in this section. Various definitions for RVEs can be found in the literature. For listings and literature reviews I want to refer to Gitman et al. [7] and Stroeven et al. [23]. Just the conclusion of relevant key findings shall be mentioned:

- Hashin [11]: An RVE must be sufficiently large to representatively depict the microstructure.
- Evesque [5]: In order to not homogenize macroscopic effects the RVE should be small enough.

Determination of an optimal RVE is not trivial. As computational costs and simulation time are crucial one has to find the optimal balance. The optimum depends on the RVE size and as well on simulation parameters, e.g. mesh fineness and particle number, which are mentioned in detail in section 2.2.3.3. The aim of the simulation with *LIGGGHTS®* is the generation of the initial packings. These need to be sufficient dense packed for the simulation in *Abaqus CAE - Simulia™*. Later the packings are inserted into the *Abaqus CAE - Simulia™* environment where the compression and yield tests are carried out.

2.2.2 Generation of the RVE with LIGGGHTS®

For extensive parameter studies various initial packings (RVEs) need to be generated. Form and size of particles determine the final size of a packing with given density. Therefore different particle shapes (Table 2.1) and particle numbers demand individual initial packing parameters.
This initial packing should fulfil following criteria:

- evenly dispersed particles
- randomly distributed particles
- particles with same size and shape (mono-disperse)
- easy to implement different shapes and sizes of particles
- roughly no overlaps between particles
- final packing should be dense packed, but not compressed
- fast and efficient generation of packings

2.2.2.1 Generation of the Initial Fibre/Multisphere

Basis of the explained procedure in this section are the bachelor theses of Segner [20] and Huber [14]. The initial fibre generation and location determination of the particles in the RVE are further developed and modified.

The cellulose fibres are modelled as multispheres in *LIGGGHTS®*. These multispheres are composed out of a set of spheres which are partially overlapping and linked together to mimic a cellulose fibre [20]. The initial multisphere is modelled with a *python* script, and depending on the input parameters (length, diameter, revolution and overlap of neighbouring spheres) outputs the set of all center coordinates of the spheres. Additionally three small spheres, the so called orientation spheres, are located around the center of the first sphere. Aim of these orientation spheres is to specify the rotation and location of the multisphere when transferring the initial packing to the *Abaqus CAE - Simulia™* environment [14]. Therefore every orientation sphere is displaced in a different direction in space (x,y or z). In this work a displacement of half the radius of one sphere is being chosen. The resulting multisphere represents an initial fibre which is set arbitrary times into the *LIGGGHTS®* simulation to fill a box with the chosen number of particles. The box shrinks till a dense packing of the multispheres is reached, which realizes the RVE.

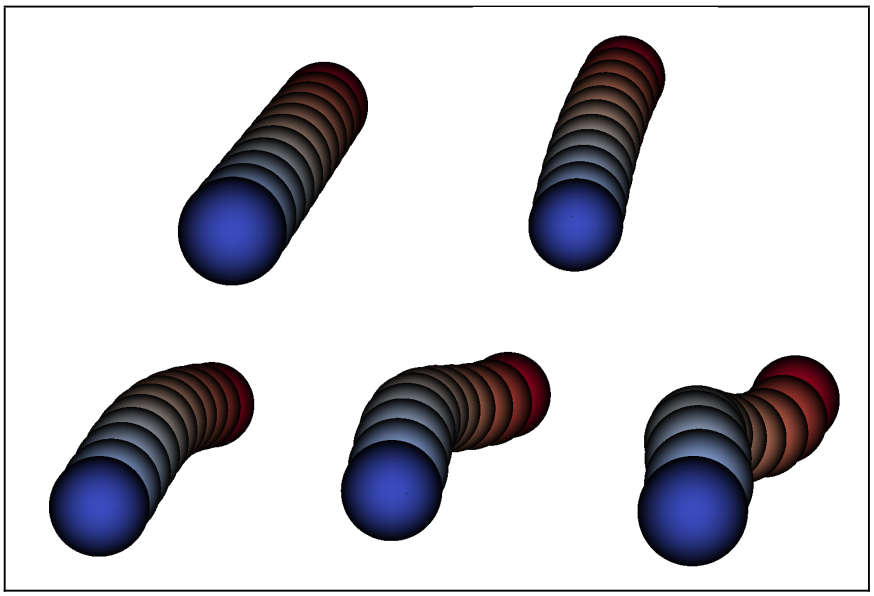

Figure 2.2: Examined particle shapes generated as multispheres in LIGGGHTS®, different revolutions, top row (left to right): 0.0 and 0.25 revolution , bottom row (left to right): 0.5, 0.75 and 1.0 revolution. All fibres have the same radius r (Table 2.1).

2.2.2.2 Material & Simulation Parameters

To inhibit huge overlaps of the particles during DEM simulation, the sphere properties are aligned with following material and simulation properties shown in (Table 2.2). The material properties density ρ, Poisson's ratio ν, coefficient of restitution ϵ, frictional coefficient μ and Young's Modulus E are kept constant throughout all simulations. The initial velocity is Gaussian distributed with a velocity mean of zero and a velocity standard deviation of Δv. A force is set on every sphere directing towards the center of the

box. The force F is set constant, but depending on the sphere location it is factorized with the distance to the center (section 2.2.2.3).

$$t_{sim} = \sqrt{\frac{2 * (l_0 - l_e)}{a_{box_{deformation}}}} \tag{2.2}$$

$$\Delta t = timefac * \frac{\pi * r}{0.1631 * \nu + 0.8766} * \sqrt{\frac{\rho * 2 * (1 + \nu)}{E}} \tag{2.3}$$

Equation (2.2) expresses the overall simulation time t_{sim} depending on the decrease of the box size and the box deformation acceleration, whereas the time increment of every simulation step Δt is chosen by following Equation (2.3). This equation depicts the Rayleigh time for granular systems factorized with the time factor $timefac$. Which is varied in the given parameter range (Table 2.2) depending on the stability of the simulation.

Table 2.2: Material properties (ρ, ν, ϵ, μ, E) and parameters (Δv, F) which are set constant for RVE generation in DEM. The timefactor $timefac$ is varied.

Constants & Parameters		
ρ	1300	$[\frac{kg}{m^3}]$
ν	0.3	$[-]$
ϵ	0.99	$[-]$
μ	0.1	$[-]$
E	$5 * 10^{12}$	$[Pa]$
Δv	1	$[\frac{m}{s}]$
F	2	$[N]$
$timefac$	0.06 – 0.006	$[-]$

In terms of efficiency an appropriate size of the initial box is important. The smallest possible box for 50 multispheres at the inserting step and the sufficient dense final box are found by trial and error procedure (Table 2.3). The initial and final size for the other particle numbers is calculated by keeping the volume of the box to volume of the particles ratio constant. Based on the initial box size with 50 multispheres the box size for 100 multispheres can be calculated. Equation 2.4 depicts the mathematical expression for this relation. All box sizes for packings with other particle numbers can be determined according to this equation.

$$l_{0_{100}} = l_{0_{50}} * \sqrt[3]{\frac{100}{50}} \tag{2.4}$$

Table 2.3: Initial length l_0 and final length l_e of the simulation box for 50 multispheres.

particle length$[m]$	$l_0[m]$	$l_e[m]$
0.3	1.5	0.6

2.2.2.3 Simulation Procedure in *LIGGGHTS®*

To guarantee evenly dispersed and randomly distributed multispheres the desired quantity of multispheres is set in a box with initial size l_0, periodic boundary conditions and the origin in the center of the box. The orientation and location of the multispheres are randomly distributed and every sphere obtains a Gaussian distributed initial velocity v in a random direction (Figure (2.3) right). The box shrinks towards the origin till the final size l_e is reached. Since the box's surfaces get smaller and the multispheres are located with higher probability on the outer box areas, the multispheres might assemble in the outer region of the box and do not disperse evenly. To circumvent fine and tedious adjustments of the deformation speed and initial velocity two additional conditions are introduced to avoid this issue. First condition sets a force F on every sphere directing towards the center of the box. The force is multiplied by the distance of the sphere to the center $l_{particle\ to\ center}$ (Equation 2.5, Figure (2.3) left). The second condition adjusts acceleration of the deformation of the box $a_{box_{deformation}}$ to the maximum occurring acceleration of a sphere a_{Sphere} located on the outer boundary. This relation is described by Equation (2.6). On the boundary of the box the force acting on a sphere is multiplied by its distance from the center, which is half the initial box size. Resulting box deformation acceleration allows for rough estimation of the derivation of the incremental box displacement Δx_{box}, neglecting the randomly distributed initial particle velocity (Equation (2.7)). Multisphere assemblies are inhibited by aligning these two accelerations.

$$F_{Sphere} = F * l_{particle\ to\ center} \tag{2.5}$$

$$a_{Sphere} = \frac{F * \frac{l_0}{2}}{\rho * \frac{4}{3} * r^3 * \pi} = a_{box_{deformation}} \tag{2.6}$$

$$\Delta x_{box} = \frac{-a_{box_{deformation}}}{2} * t_{sim}^2 \tag{2.7}$$

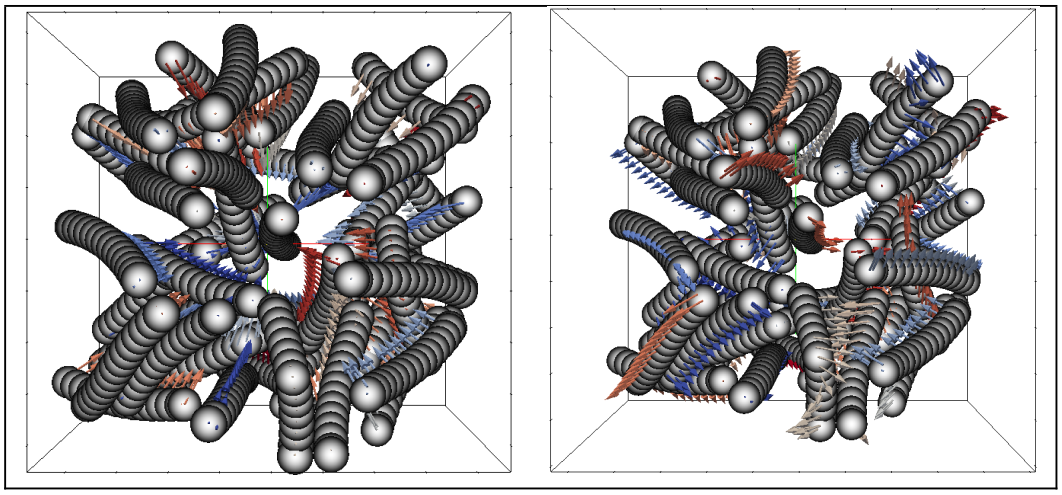

Figure 2.3: Initial arrangement of multispheres in box; vectors indicate the direction of the force acting on each sphere (left) and indicate the direction of the initial velocity (right).

2.2.3 MPFEM Modelling with Abaqus CAE - Simulia™

With MPFEM, powder simulation and modelling seems to be within ones reach. Considering discrete particles with an individual finite element mesh offers the opportunity to widen the horizon of powder simulation.
The hurdles of powder compaction process simulation not only arise from the difficulty of setting up a material model which connects stress and strain (in classical FEM) but also taking particle deformation into account. Moreover implementing inter particle contacts, for example cohesion, is problematic in DEM.
Due to the MPFEM approach these hurdles can be overcome. The simulation procedure, concept and some background informations are outlined in this section. For detailed description and a deeper insight into this concept I want to refer to the work of Loidolt et al. [17].
Recent works in the literature mainly consider powder as spherical particles, either three dimensional as spheres or two dimensional as circles. This paragraph gives a short overview of some MPFEM approaches dealing with powder compression. Some as well determine yielding of the powder probes:

- Zhang [28]: Deals with the closed die compaction process of mono-sized particles (2D) containing a composite mixture of soft and hard particles and examines the compression behaviour.
- Zhang et al. [29]: Analyse the single action die compaction process of copper in 2D with a special glance on the characteristics of the compaction processes, deformation and densification mechanisms.

- Huang et al. [13]: Describe the densification process, mechanisms and dynamics of poly-disperse (binary) Al & SiC composite powders (2D).
- Harthong et al. [10]: Mono-sized sphere (3D) assembly compression and a method to probe yielding was proposed to micromechanical interpret and understand the micromechanical phenomena.
- Gustafsson et al. [8]: The compression of iron ore pellets was examined with the confined compression test of 2D spheres with statistically distributed size, shape and material properties. A fraction criterion was introduced. Determining the stress inside the particles estimates the prediction of failure.
- Abdelmoula et al. [1]: Study the plastic flow of isotropic and closed die compaction and a method for probing yield surfaces is proposed.

However, the simulation concept used for this work [17] is based on a RVE and uses another kind of periodic boundaries to introduce periodic boundary conditions and circumvent the influence of wall effects. Further differences to the mentioned studies is the introduction of non-spherical particles. Particles resembling fibres, are introduced in the simulation box and the influence of length and rotation is examined after a parameter study. In the next sections the simulation set-up is explained reasonably. The parameters and material properties are outlined and a short overview over the simulation procedure in *Abaqus CAE - Simulia*™ is given.

2.2.3.1 Simulation Setup/ Environment

In section 2.2.1 the aim of an RVE is already stated as well as the generation of initial packings with *LIGGGHTS*®. Subsequently in the *Abaqus CAE - Simulia*™ environment a periodic simulation box containing these particles, the initial packing, is introduced. When the particles initial packing is transferred from *LIGGGHTS*® into the *Abaqus CAE - Simulia*™ simulation environment, they are formed out of one part instead of an assembly of spheres. The location of the particles is determined with the center point of the first sphere. With the coordinate information of the orientation spheres the rotation of the fibre in space is found. Particles touching the upper boundary of the periodic box are shifted to the lower boundary. After the meshing of the particles the fibres on the boundary are duplicated (one, three or seven times) and transferred to the linked boundaries (Figure 2.4), respecting the periodic boundary condition. E.g. a particle on the edge needs to be duplicated three times to fulfil the periodicity condition (Figure 2.4, center). Not until then particles ranging out of the simulation box are cut and protruding elements are deleted.

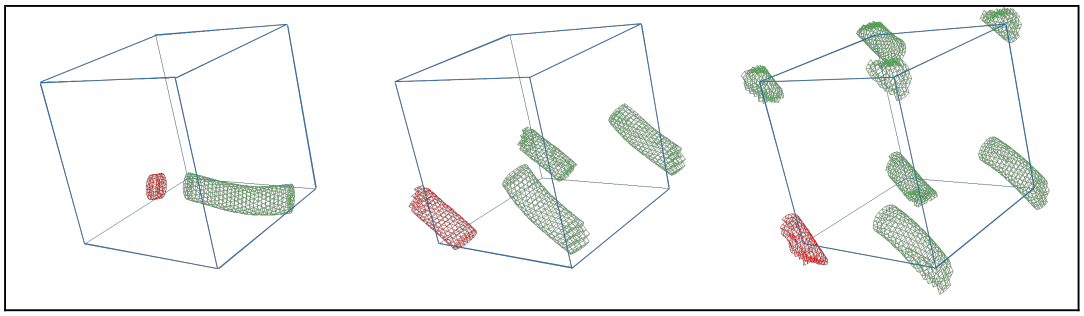

Figure 2.4: The red coloured mesh shows the initial already cut particle which lies on a boundary face (left), on the edge (center) or in the corner (right). To fulfil the periodic boundary condition the green coloured particles are duplicates. The periodic box is shown in blue color.

Loidolt et al. [17] found that an extra layer around the periodic box of around half a particle radius r diminishes boundary effects. As in this study no spheres, but elongated particles are examined a slightly thicker additional layer Δx_{add} (Equation 2.8) is used.

$$\Delta x_{add} = 2 * r * frac_{add,layer} + \frac{1}{4} * l_{element} \tag{2.8}$$

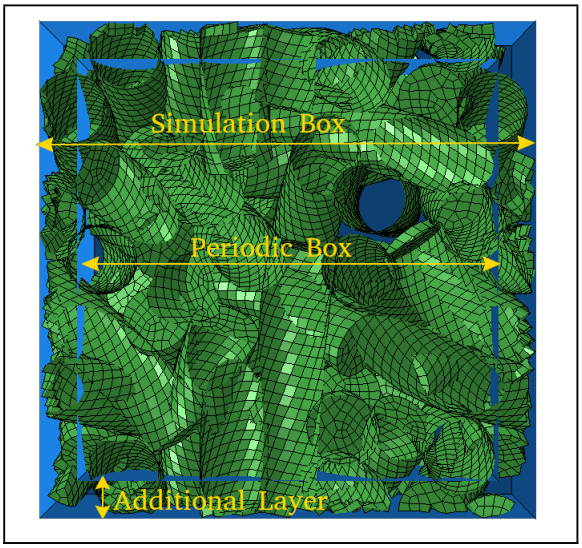

Figure 2.5: View on RVE with artificial added periodic and simulation box (blue) for demonstration reasons. The green meshed fibre particles are located in the simulation box. The periodic box is extended with an additional layer to diminish boundary effects. The particles in the simulation box are the basis for later simulations.

This additional layer not only depends on the radius r but also on the size of one element $l_{element}$ and an additional-layer-fraction parameter $frac_{add,layer}$. In this additional layer, particles within the periodic box can reach into the additional layer, whereas particles which would lie just outside the periodic box are not duplicated. Additionally, all

remains of fibres with less than three elements are eliminated, as they do not influence the simulation procedure. Figure 2.5 shows the periodic box with the additional layer, which forms the basis for later compression and reloading procedures. Throughout all simulations an additional-layer-fraction parameter $frac_{add,layer}$ of 0.5 is chosen.

Boundary Condition, Constraints and Coupling

Every particle on the boundary is given a reference point in the particles center. A defined number of nodes of the particles which lie in the additional layer are coupled with this reference point. The coupling is enabled by distributed coupling, which distributes loads from the reference point to the coupled nodes or vice versa. Opposite particles reference points are constrained via linear constraint equations for all three translational and rotational degrees of freedom. Defined three auxiliary nodes enable the controlled displacement, as their displacement is included in the linear constraint equations. The overall boundary condition concept allows for periodic boundary conditions over the RVE, but the concept allows for single particles to have traction boundary conditions which in total results in a mixed-Dirichlet-Neumann boundary condition [17].
To sum up this paragraph and emphasise its importance: Kinematic constraining of the auxiliary nodes to the reference points of boundary particles enables deformation of the box. The reference points of particles are linked via distributed coupling with their nodes. These conditions enable incremental deformation of this non-linear system, subsequently solving of the equations and therefore incremental calculation of the nodal position.

Contact Modelling

As already mentioned with the MPFEM inter-particle contacts can be modelled. In *Abaqus CAE - Simulia*™ various arbitrary contact models can be implemented. In this work just one contact model is examined, which takes repulsive force, friction force and cohesion force into account. Implementation of different contact models is proposed for further works. As the model is similar to the one used in [17] the contact model itself and the implementation details are just outlined.
The contact force of a node on the slave surface arises from the contact stress and associated nodal contact area. The nodal contact stress is computed in the implemented user defined subroutine *VUINTERACTION* in *Abaqus CAE - Simulia*™ [21]. Two slaves contact forces are weighted equally and the resulting contact force is received from linear combination of the pure forces of the master slaves.
The distance normal to the master surface δ_N (Figure 2.6, left) has positive values for overlap/penetration and negative values for no physical contact. The normal stress is computed concerning this normal distance δ_N and is linearly dependent on the contact normal stiffness k. The tangential displacement δ_T results in the tangential contact stress.

Both stresses may be damped with a damping factor d which acts as a damper for the system depending on the normal relative velocity $\dot{\delta_N}$ and tangential relative velocity $\dot{\delta_T}$. Aim of the damping factor is to stabilise the contact forces and inhibit oscillation. The interaction length δ_0 determines the distance from which onward cohesion contact forces occur. With decreasing master-slave-surface distance the cohesion force increases linearly. As the surfaces touch each other the cohesion force $\sigma_{coh_{max}}$ remains constant, independent on the penetration. The evolving repulsion and cohesion stress over surface distance is sketched in the right picture of Figure 2.6. The friction force occurs when the surfaces are in contact. It depends on the tangential displacement δ_T and is limited by a maximum friction stress. The maximum friction stress results from the repulsive stress times the coefficient of friction.

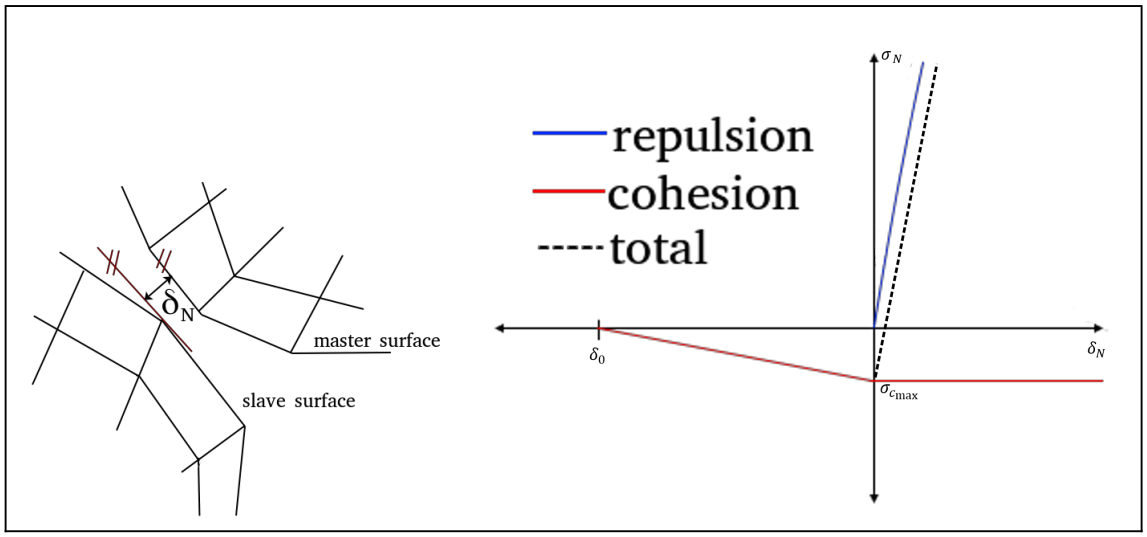

Figure 2.6: The normal distance δ_N between master surface and slave surface determines force intensity (left), schematic course of repulsion and cohesion stress as function of the normal distance δ_N , positive δ_N values are interpreted as overlap and damping effects are neglected (right).

Table 2.4: Contact model properties.

Constants & Parameters		
μ	0.2	$[-]$
δ_0	$0.01 * 2 * r$	$[m]$
d	$5 * 10^8$	$[\frac{Pa*s}{m}]$
k	$5 * 10^{12}$	$[\frac{N}{m}]$
$\sigma_{coh_{max}}$	$1 * 10^8$	$[Pa]$

Stress, Strain & Yield Criterion

A short overview over the determination of the stress, strain and the yield point is given in this section. The most important assumptions and details are outlined. For additional and detailed descriptions I may refer to the work of Loidolt et al. [17].
As already mentioned three auxiliary nodes are defined in the simulation environment. Every auxiliary node is assigned to one direction in space, either x, y or z. The nodes are kinematically constrained with the reference points of the boundary particles and enable controlled displacement. Furthermore, they are essential for the stress, strain and yield point determination.
To determine the yield point a plastic deformation criterion for the powder is required. As only small strains occur during the yielding the small strain theory is assumed. This theory implies a coincidence of the first Piola-Kirchhoff stress tensor with the Cauchy stress tensor, Equation (2.9). The three force vectors F_x, F_y and F_z of the auxiliary nodes and their components are necessary to compute the stress tensor.

$$\boldsymbol{\sigma} = \begin{bmatrix} \frac{F_{xx}}{A_x} & \frac{F_{xy}}{A_x} & \frac{F_{xz}}{A_x} \\ \frac{F_{yx}}{A_y} & \frac{F_{yy}}{A_y} & \frac{F_{yz}}{A_y} \\ \frac{F_{zx}}{A_z} & \frac{F_{zy}}{A_z} & \frac{F_{zz}}{A_z} \end{bmatrix} \tag{2.9}$$

The strain tensor can be obtained from the displacements of the three auxiliary nodes Δu_x, Δu_y, Δu_z and their components. Equation (2.10) shows the mathematical expression for the strain tensor, where X, Y and Z are the box lengths in the respective direction.

$$\boldsymbol{\epsilon} = \begin{bmatrix} \frac{\Delta u_{xx}}{X} & \frac{1}{2}\left(\frac{\Delta u_{xy}}{X} + \frac{\Delta u_{yx}}{Y}\right) & \frac{1}{2}\left(\frac{\Delta u_{zx}}{Z} + \frac{\Delta u_{xz}}{X}\right) \\ \frac{1}{2}\left(\frac{\Delta u_{xy}}{X} + \frac{\Delta u_{yx}}{Y}\right) & \frac{\Delta u_{yy}}{Y} & \frac{1}{2}\left(\frac{\Delta u_{yz}}{Y} + \frac{\Delta u_{zy}}{Z}\right) \\ \frac{1}{2}\left(\frac{\Delta u_{zx}}{Z} + \frac{\Delta u_{xz}}{X}\right) & \frac{1}{2}\left(\frac{\Delta u_{yz}}{Y} + \frac{\Delta u_{zy}}{Z}\right) & \frac{\Delta u_{zz}}{Z} \end{bmatrix} \tag{2.10}$$

The yield stress indicates the end of elastic behaviour and the onset of plastic deformations. Loidolt et al. [17] introduced in their work a universal yield criterion. They proposed an equivalent plastic strain ϵ_{pl} which indicates plastic deformation when an equivalent plastic strain of 0.002 is reached. The equivalent plastic strain ϵ_{pl} (Equation (2.11)) depends on the elastic strain tensor $\boldsymbol{\epsilon_{el}}$ and the strain tensor at the yield point $\boldsymbol{\epsilon_{yp}}$. The elastic strain tensor $\boldsymbol{\epsilon_{el}}$ is determined from the displacement of the RVE during the unloading step.

$$\epsilon_{pl} = \sqrt{\frac{2}{3} * \boldsymbol{\epsilon_{yp}} : \boldsymbol{\epsilon_{yp}}} - \sqrt{\frac{2}{3} * \boldsymbol{\epsilon_{el}} : \boldsymbol{\epsilon_{el}}} \tag{2.11}$$

2.2.3.2 Simulation Procedure in *Abaqus CAE - Simulia™*

Initial Hold Step

Since in the initial packing the particles slightly overlap due to small differences of the multisphere fibres (in *LIGGGHTS®*) and the meshed fibres (in *Abaqus CAE - Simulia™*) transition no deformation is applied during this step. The contact stiffness is linearly ramped from zero to the final value, to inhibit high local contact forces and allow small rearrangement of the fibres in the packing to lower the overlaps (Figure 2.7 top left and right). This step lasts five seconds, in terms of simulated time.

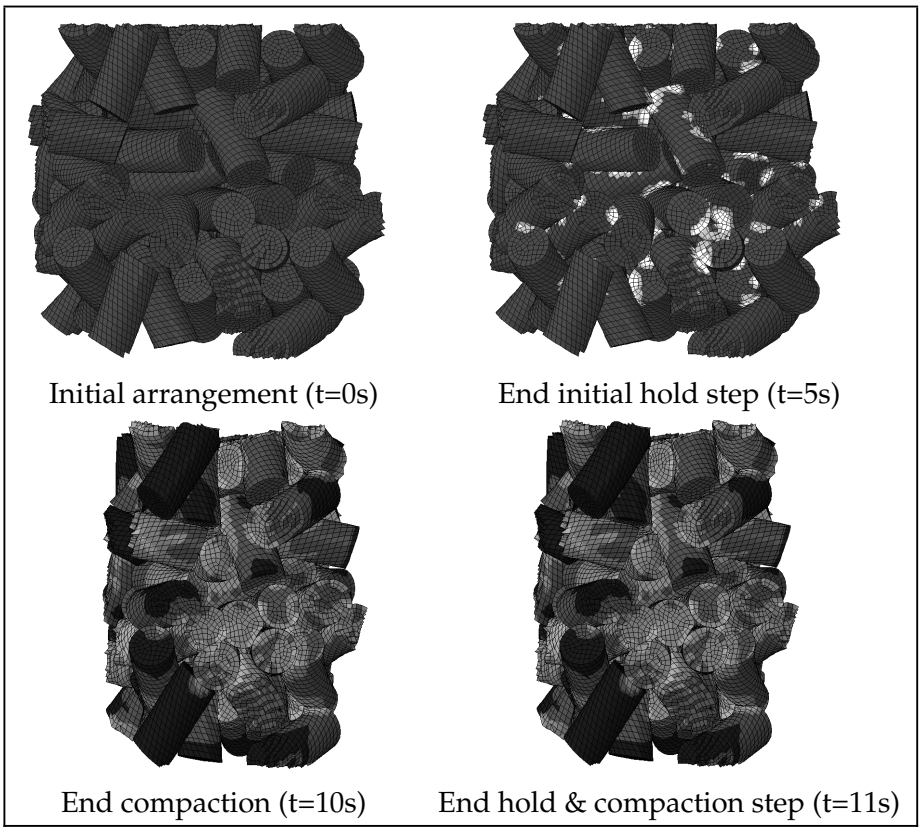

Figure 2.7: Top view on RVE with 50 particles. Snapshots from beginning and end of the initial hold step (top row, left to right), compaction and hold (bottom row, left to right) shown in chronological order. Colouring represents the maximal (white) and minimal (black) occurring stress in the RVE.

Compaction Step & Hold

In the compaction step deformation is applied to the RVE. After the step time of five seconds the compaction to the predefined relative packing density is realised with deformation-controlled uni-axial compression. The incremental deformation of the packing is linearly ramped up till half of the step time is reached and subsequently ramped down till the

tenth second. Ramping up and down of the incremental deformation is applied to avoid high accelerations. After the compaction (Figure 2.7 bottom left) one second of holding (Figure 2.7 bottom right) is applied. During this time the boundaries are kept constant. If some potential oscillations arise during the compaction step, they can be damped during this holding time.

Unloading Step

At the beginning of the unloading step the deformation-controlled load control switches to force controlled mode. During this step the load is linearly ramped down to 0.1 MPa. This residual stress is to avoid disaggregation of the RVE, which may occur at low cohesion. This RVE state is the basis and reference state for further yield studies. This step lasts five seconds.

Reload/ Yield Step

The yield step may be repeated more times to test the yielding in different directions. Every yield test starts with the reference RVE received from the unloading step. To get a precise result from the yield test of one certain direction, the yielding is tested in three iterative steps. The direction of the load may vary in arbitrary directions. To get an idea of this procedure in the following paragraph it is assumed to test the yielding in x-direction and to test the compression strength:
In the first iteration in the yield step the stress towards the RVE in x-direction is ramped up in such a way to certainly reach the yield point. Then the second iteration to determine the yield point is started. The RVE configuration from a defined state before the first yielding occurred is taken as initial configuration for the second iteration. The second yield iteration is then started with a load ramp velocity smaller than the ramp velocity for the first time and lasts till yielding occurs. The initial configuration for the third and last yield iteration is again taken from the second iteration. The third yielding proceeds a defined state before the second yielding occurred and with a slower ramp velocity. It is necessary to ramp the load slow enough to not having inertia effects influencing the final result. The mentioned procedure with three iterations is the procedure for testing one yield direction. For every yield test direction the yield point is determined after each third yield trial. This procedure arose due to maximization of accuracy and efficiency [17]. Every yield iteration's simulated time lasts a maximum of five seconds, but ends when the yield point is hit.

2.2.3.3 Parameters & Material Properties

During the overall simulation particles are modelled as elasto-plastic body and the material properties (e.g. density and Young's Modulus) of the particles are the properties of copper. The neglect of particle breakage might be relevant when high deformation occurs. The properties of copper for the particles are used instead of the material properties of MCC, as in the first step the effect of the geometrical properties of the fibres (length, diameter and revolution) on the overall material behaviour is examined. In subsequent studies it is proposed to change the material properties to the properties of the MCC. Simulation parameters, like solver time step, mesh fineness, mass scaling, sufficient particle number for the RVE have to be determined with parameter studies. In this work every parameter study is realised one time although the selection of the parameters with efficient and stable solving behaviour is an iterative process, since they effect each other. Since mass scaling increases the time step size and is valid as long as no inertia effects occur (quasi static model) it enhances the efficiency. Shortly summarized mass scaling is the artificial increase of the particle density with a mass scaling factor $fac_{scale\ mass}$. For further details of mass scaling in explicit FEM see Chung et al. [2] and tailored to this work see Loidolt et al. [17].

Material Properties

As mentioned above, the material properties of copper are chosen. Since changing too much inhibits direct comparison between the previous work of Loidolt et al. [17] where the spheres are as well modelled with the material properties of copper. In Table 2.5 the material properties are summarised.

Table 2.5: Material and yield properties of copper used as particle material: density ρ, Young's Modulus E, Poisson's Ratio ν and the stress σ dependent on the plastic strain $\epsilon_{plastic}$.

Material Properties		
ρ	8920	$[\frac{kg}{m^3}]$
E	115	$[GPa]$
ν	0.34	$[-]$
$\sigma\,[Mpa]$		$\epsilon_{plastic}$
	150	0.00
	250	0.06
	300	0.30
	350	1.00
	400	2.50
	450	5.00

Simulation Parameters - Convergence study for the RVE

Determining a convenient RVE requires elaboration of appropriate simulation parameters, which guarantee the maximum balance between accuracy and computational effort. The convergence study results from the work of Loidolt et al. [17] are taken as initial values for the simulation parameters , see Table 2.6.

Table 2.6: Results from the convergence study of spheres of Loidolt et al. [17] which are taken as initial values for fibre shaped particles convergence study.

Initial Values for Simulation Parameters		
particle number RVE	50	$[\frac{No.\ particles}{RVE}]$
Δt_{solver}	$1 * 10^{-4}$	$[s]$
$fac_{scale\ mass}$	$1 * 10^{4}$	$[-]$

The convergence of the mesh fineness, which is parametrised with the number of element per fibre diameter d, is elaborated in the first parameter study . The particles are meshed with eight-node linear brick (C3D8 [21]) elements. When the optimal element number is found, the convergence of particles inside the RVE is examined. Sufficient particles are required in the RVE to homogenize microscopic effects and yield the macroscopic properties. Later the solver time step size Δt_{solver} is varied. Although it strongly correlates with the mass scaling the convergence study is executed just once. Next the mass scale factor $fac_{scale\ mass}$ is varied. The examined parameter range is shown in Table 2.7. When all convergence studies are finished and the optimum parameters are obtained the geometrical properties of the fibres are changed and its effects examined. Although the influence of other parameters such as relative density after compaction, cohesion strength and friction coefficient might be of interest the focus of this work lies on geometrical influences.

Table 2.7: Mesh fineness, particle number inside RVE, solver time step size and mass scale factors variation range to study the convergence behaviour.

Variation Range Parameters for Convergence Study		
mesh fineness	3 – 7	$[\frac{elements}{d}]$
particle number RVE	50 – 300	$[\frac{No.\ particles}{RVE}]$
Δt_{solver}	$5 * 10^{-6} - 2 * 10^{-4}$	$[s]$
$fac_{scale\ mass}$	$5 * 10^{3} - 10^{7}$	$[-]$

Chapter 3

Results & Discussion

The focus of this section lies on the convergence study results and the effects of different geometrical shapes of the fibres on the yield strengths, in terms of the number of revolutions. Besides the already mentioned contact model parameters (Table 2.4) and material parameters (Table 2.6) the *Abaqus CAE - Simulia*™ environment needs some more input parameters which are depicted in Table 3.1. Although varying the final relative compaction density and the effects on the strengths might be of interest we keep this parameter constant throughout all simulations. A final relative density of 0.85 after the compaction step is chosen, as this relative density guarantees a compaction of all packings without high deformations of the elements and results in sufficient high strengths of the RVE. The tracking thickness specifies the maximum distance between two surfaces from which onward contact is assumed and the contact model is evaluated. To certainly detect all contacts the additional length of one percent of the radius is added to the interaction length δ_0.

Table 3.1: Simulation parameters for the *Abaqus CAE - Simulia*™ environment which are set constant throughout all simulations.

Simulation Parameters for *Abaqus CAE - Simulia*™ environment		
tracking thickness	$\delta_0 + 0.01 * r$	$[m]$
final relative compaction density	0.85	$[\frac{V_{particles}}{V_{box}}]$

3.1 Convergence Studies

The applicability of a convenient RVE is analysed with the aid of observing the convergence behaviour of the uni-axial yield strength as function of the simulation parameters. In the first step the minimum mesh fineness is examined, then the particle number inside the RVE is varied and the minimum applicable number of particles is identified. Subsequent to the convergence study of the solver time step size the convergence behaviour of the mass scaling factor is investigated. Higher numbers of particles inside the RVE lead to lower possible mass scaling factors. Furthermore the solver time step size influences

the mesh fineness for a stable simulation, which emphasises the need of an iterative procedure to determine proper simulation parameters. However these convergence studies take a lot of time and the context of this master thesis does not allow for this iteration process. Every simulation parameter is just determined once and these parameters are not chosen perfectly, yet quantitative results can be obtained.
All following simulations result from an uni-axial compaction in x-direction in the compaction step. If not stated differently the compression and tension strength result from a yield testing in x-direction. The isostatic strength is tested with equal loadings in all three directions, if not stated differently isostatic strength of compression is tested. For all yield strength results the tensile strength has positive values whereas the compression strength has negative values.

3.1.1 Mesh Fineness

The mesh fineness parameter defines how fine the fibres are resolved. On the one hand higher element numbers result in a finer mesh, but on the other hand the total simulation time increases as more equations need to be solved. For all mesh convergence studies Table 2.6 lists the values for the solver time step size and mass scaling. Figure 3.1 shows the uni-axial strengths depending on the element number per fibre diameter of one initial RVE with 50 particles.

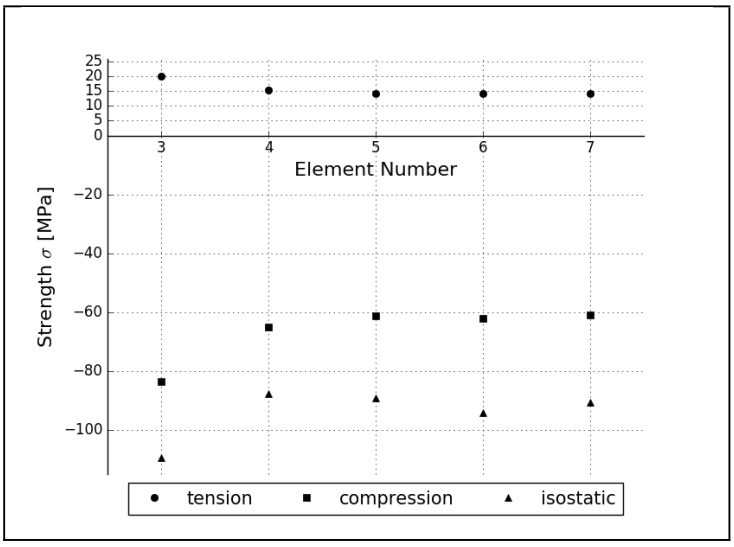

Figure 3.1: Mesh fineness convergence behaviour of one RVE containing 50 particles. The initial packing was kept the same throughout this mesh fineness convergence study.

The element size is varied between three and seven elements per diameter. The uni-axial yield strength for a mesh fineness of three outranges the strengths of the other element numbers. In the element number range from four to seven the strengths do not vary

significantly, only for isostatic compression the strength increases slightly for five and six elements. Since the compression and tension strengths stay approximately constant from four elements onwards and while being aware of strongly increasing simulation time with the element number, an element number of four is chosen for following studies.
Figure 3.2 depicts strengths of three different RVEs (unfilled markers) compared to the strength averaged over all three different simulation results (filled markers). One can clearly derive that although the single results differ significantly from the averaged results they follow a schematic curve, which flattens with higher element numbers. The particle number inside the RVE may have and influence on the resulting strength, and it may as well influence the resulting strengths in the yield study. Therefore the mesh fineness convergence study should be repeated with the sufficient high number of particles found in the particle number convergence study. The significant difference between the single results of studies with the same element number may as well arise from the fact that the initial packings differ in the initial relative packing density.

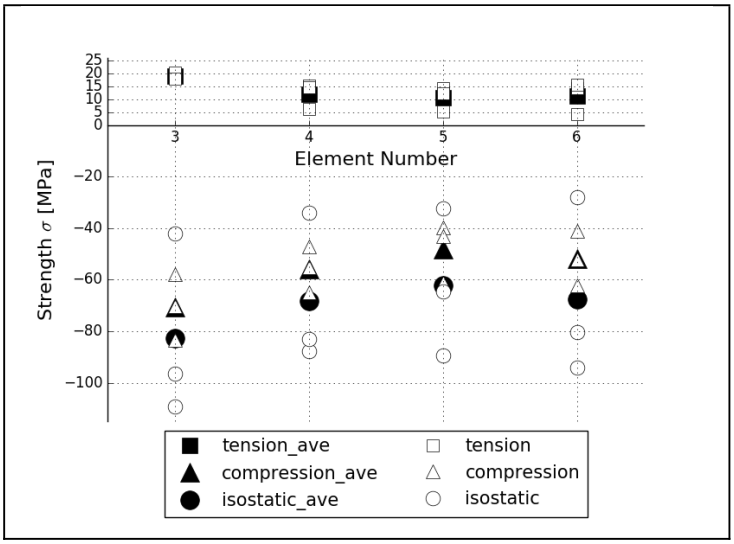

Figure 3.2: Unfilled markers show individual simulation results from different initial RVEs, whereas filled markers represent the averaged strengths.

Figure 3.3 shows the cross section of RVEs with different element numbers and emphasizes the choice of four elements per diameter. Obviously a mesh fineness of three is too coarse to show local stress characteristics. The stress distribution of the RVE with a mesh fineness of seven may be taken as reverence RVE for high resolved stress characteristics. Compared to the other RVEs an adequate detailed stress profile over the cross section from a mesh fineness of four onward is obtained. The stress distribution in the RVE with four elements per diameter is sufficiently resolved to depict stress characteristics.
The particles which are additionally inserted in the additional layer can be clearly distinguished from the others. These particles are in Figure 3.3 boundary particles located on

the edges of the RVE and coloured dark as they take in less stress. Their aim is to improve the stress distribution in the periodic boundary region (section 2.2.3.1).

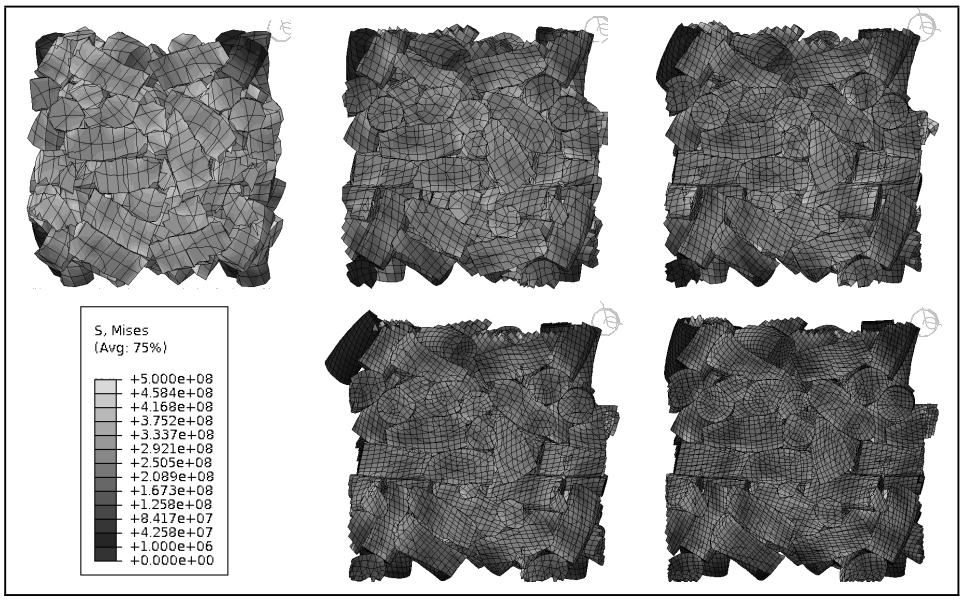

Figure 3.3: Cross sections of one RVE with 50 Particles after the compaction step. Top row (left to right) shows RVEs with three to five elements per diameter and bottom row (left to right) shows element numbers of six and seven per fibre diameter. Colouring refers to highest (white) and lowest (black) occurring stress (bottom row, left).

3.1.2 Particle Number

The convergence behaviour of an RVE containing different numbers of particles is investigated in this section. The examined particle number inside the RVE ranges from 50 to 500. A high enough number of particles should be chosen to inhibit big influences of the RVE properties. However more particles lead to longer simulation time and higher computational costs. Every RVE with different particle number needs an individual initial packing. Besides the number of particles, all other parameters remain constant. In Figure 3.4 the simulation results for one particle packing per particle number is shown for illustrative reasons. The compression and isostatic strength is diverging and does not seem to converge in the examined particle number range. The tension strength seems to converge from 150 particles onwards.

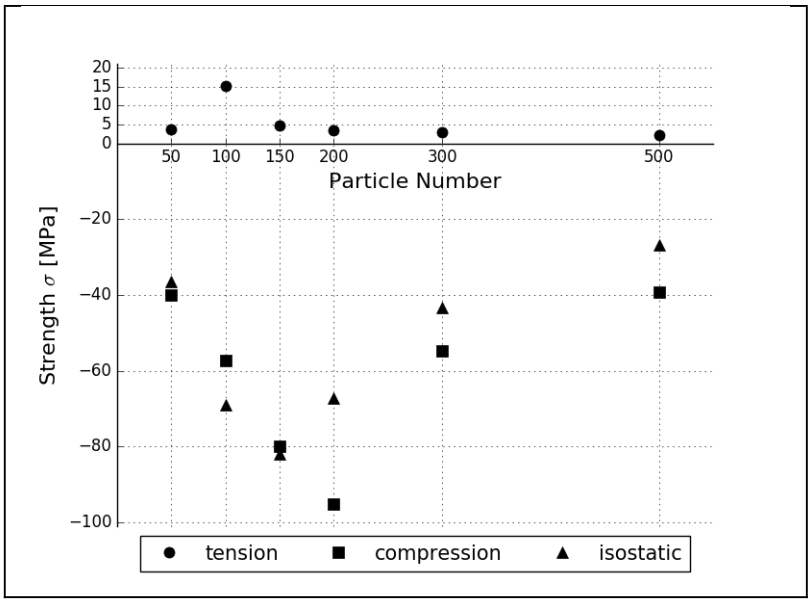

Figure 3.4: Resulting strengths for different particle numbers inside RVE. For illustrative reasons just one particle packing per particle number is depicted, as the course of the results is similar.

In Figure 3.5 the Relative Standard Deviation (RSD) of three different random packings per particle number is investigated. In our case the RSD is the standard deviation of the yield strength and is expressed as a percentage value relative to the averaged strength. As different yield test directions may indicate individual effects, averaging over all yield test directions of one particle number is not applicable. Hence every yield tests RSD is shown as a function of the particle number. It is suggested that the yield test in y- and z- direction are in a similar value range as the compaction direction in the compaction step is towards the x-direction. However, the RSD of these values do not follow this suggestion, which leads to the presumption that different initial configurations lead to this diverging effect. What might be impacting the result as well is the dissimilar relative initial packing density. Although the compaction relative density after the compaction step is the same for all simulations, the different initial relative packing densities may allow for different scales of rearrangement movements and different rate and deepness of overlapping particles. These overlaps are the basis of contact forces and stresses and subsequently the initial stress distribution and stress forces might diverge significantly for different initial packings. However, to proof this presumption, further studies are necessary.

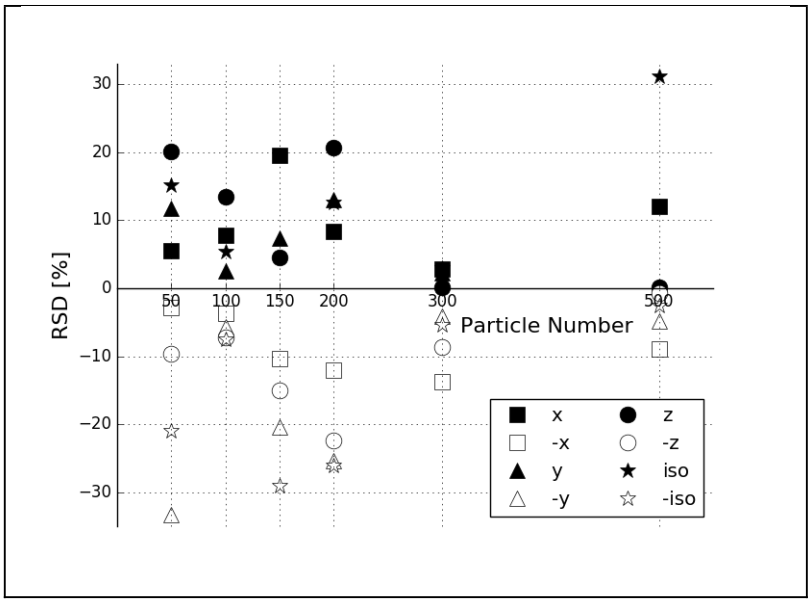

Figure 3.5: RSD of the yield strengths for three particle packings per particle number. X, y or z indicates the yield testing direction, the minus indicates compression yield testing and the plus indicates tension yield testing.

The RSD for 300 particles is for all yield test directions relative low compared to the RSD of all other particle numbers, which recommends the particle packing of 300 for further studies. However, a particle packing of 100 particles is chosen, as the RSDs of the yield strengths are not exceeding 15 percent and are compared to 300 particle packings RSD in a similar range. The initial packings with 50, 150, 200 and 500 particles have RSDs up to 30 %. Therefore their strengths may vary which is not applicable for following studies. Taking the computational time and costs into account underlines the usage of initial packings with 100 particles for further simulations.

3.1.3 Simulation Time Step

The time step size Δt_{solver} is a crucial parameter for the simulation as it strongly influences the simulation time, convergence behaviour and therefore the quality of the results. To examine the convergence behaviour one particle packing with 100 particles, a mesh fineness of four elements per diameter and 10^4 mass scale factor is used as the basis for this convergence study. The influence of time step size Δt_{solver}, ranging from $5 * 10^{-6}$ s to $2 * 10^{-4}$ s, on the resulting strengths is examined. This range was chosen because bigger solver time step sizes than $2 * 10^{-4}$ s are not stable and smaller time step sizes than $5 * 10^{-6}$ s lead to extremely long simulation times. For the Δt_{solver} of $5 * 10^{-6}$ s about two weeks of simulation time with three CPU cores are necessary to realize all simulation steps with ten different yielding direction tests. Figure 3.6 depicts the strengths versus

the solver time increment size. One can derive from the chart that the results stay about constant for all solver step sizes observed, however small deviations occur.
In particular the isostatic yield strength deviates with a standard deviation of 4.1 *MPa* around the arithmetic mean of −75.0 *MPa* which results in a RSD of −5.4 %. The tensile and compression strengths are about equally sensitive to the solver time step size. Both strengths deviate with a standard deviation of around 0.7 *MPa* and 1.9 *MPa* respectively around their arithmetic mean of 13.9 *MPa* and −54.3 *MPa*. The RSD of the tensile strength is 5.0 % and the RSD of the compressions strength is −3.4 %. Comparing the RSDs of the three yield strengths concludes that the strengths are slightly varying but a significant difference between tension, compression and isostatic yield strength can not be observed. Additionally, the maximum RSD of 5.4 % states a negligibly deviation. The biggest solver time step size of $2 * 10^{-4}$ *s* still guarantees stable simulation and convenient results. Since in later studies differently twisted particles are examined and therefore the mesh and element configuration may vary, a slightly smaller solver time step size of 10^{-4} *s* is chosen to guarantee a stable simulation.

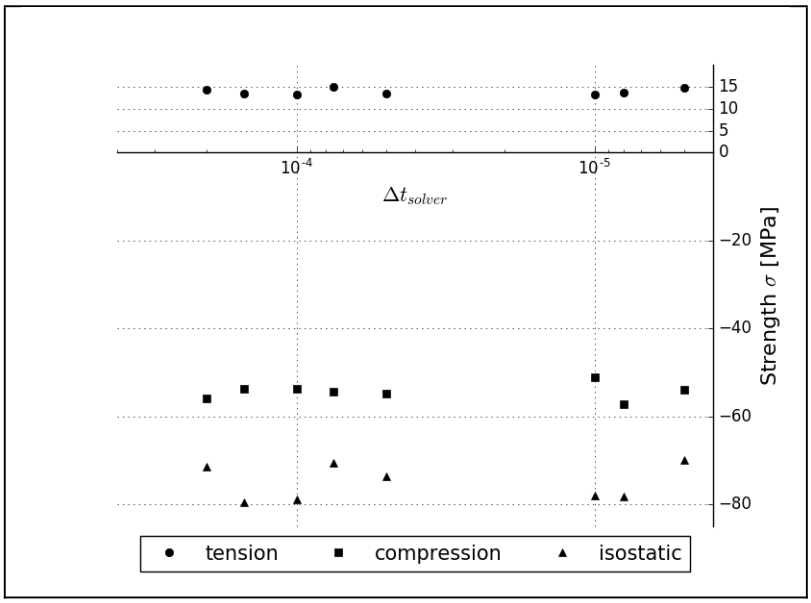

Figure 3.6: Yield strengths for one particle packing depending on the solver time step size Δt_{solver}. The x-axis is plotted logarithmically and inverse order to emphasize the convergence behaviour.

3.1.4 Mass Scaling

The convergence study of mass scaling is performed with various mass scale factors $fac_{scale\ mass}$. This factor is multiplied by the density to increase the mass of the particles and enables stable simulations and larger solver time sizes. Loidolt et al. [17] demonstrated that applying the explicit solver in *Abaqus CAE - Simulia*™ and using the mass

scaling factor, results in an applicable solver time step size and convergence behaviour. Basis for this convergence study are the results from the previously examined parameters. A packing of 100 particles with a mesh fineness of four elements per particle diameter and a solver time step size of 10^{-4} are set constant during this study. The mass scale factor $fac_{scale\ mass}$ is varied between 10^7 and $5 * 10^3$. Figure 3.7 illustrates the convergence behaviour of one particle packing with different mass scale factors $fac_{scale\ mass}$. For higher values of $fac_{scale\ mass}$ than 10^5 the strength results diverge and for 10^7 $fac_{scale\ mass}$ the compression strength is already about 10 times bigger than for 10^5 $fac_{scale\ mass}$. High mass results in inertia effects which falsify the resulting strengths. Inertia effects cause a lag of yielding, which raises the yield strengths to higher values. For $fac_{scale\ mass}$ values lower than 10^5 the strengths show a convergence behaviour. A mass scale factor of 10^4 is taken for subsequent studies. To guarantee stable simulations for differently twisted particles a mass scale factor of 10^4 is chosen and not the minimal possible mass scale factor. Loidolt et al. [17] observed in their studies with spheres the same behaviour for the mass scaling that for low mass scale factors instability problems occur. Their $fac_{scale\ mass}$ ranged down to 300 $fac_{scale\ mass}$, which could not be performed in our studies as the simulations did not succeed due to instability issues. The lowest possible $fac_{scale\ mass}$ with a time step size of 10^{-4} s is $5 * 10^3$ for the configurations of this study.

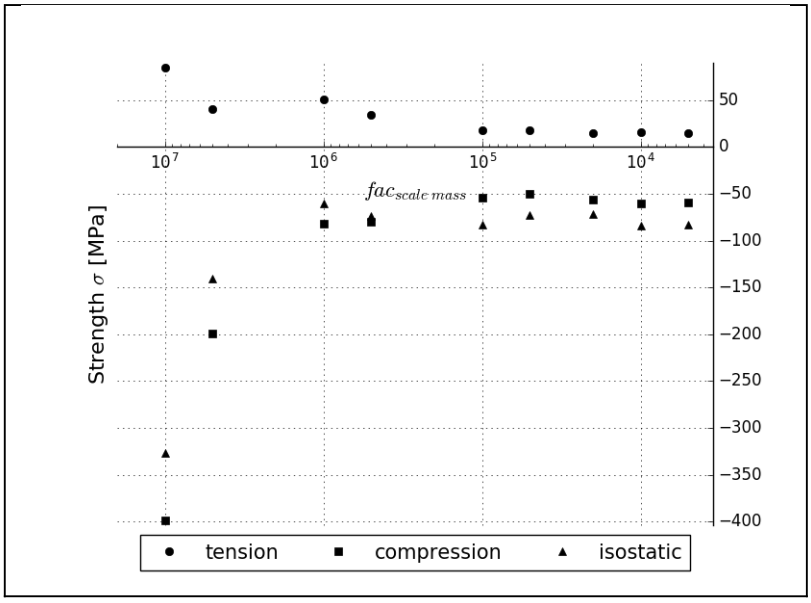

Figure 3.7: Yield strengths for one particle packing depending on the mass scale factor $fac_{scale\ mass}$. The x-axis is plotted logarithmically and inverse order to emphasize the convergence behaviour.

3.2 Particle Shape and Size

The influence of the geometrical properties of fibres in terms of the particle twist is examined in this section. The length of the particles is kept constant while the revolution (number of revolutions per fibre length) of the particles is kept constant. Twisting of particles may improve or decline the resulting yield strength.

The revolution of the particles influence the strength in different ways:

- contact area of particles
- tangling of particles
- different characteristics of stress distribution

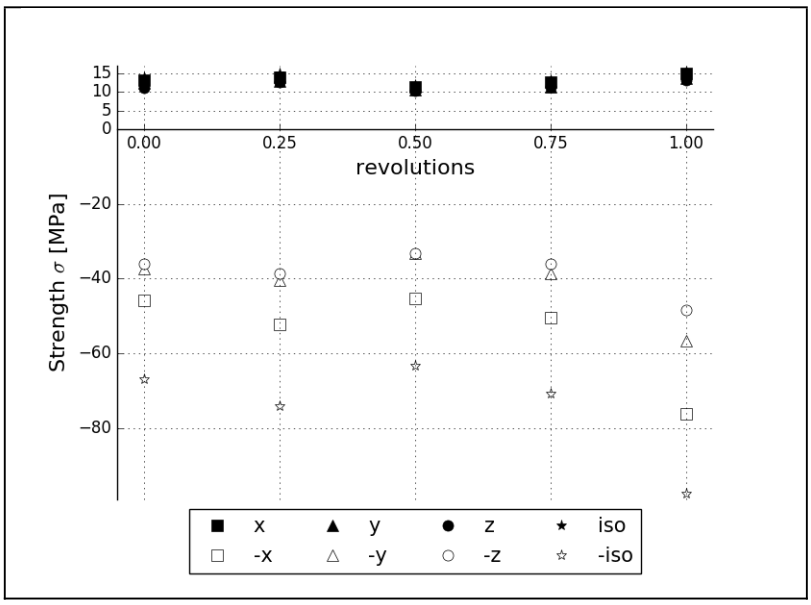

Figure 3.8: Uni-axial and isostatic yield tests in different directions to the RVE. Three different initial packings per particle revolution are tested and the averaged yield strengths are shown.

One would assume that with increasing revolution the strength increases as the particles tangle and have a higher contact area. Figure 3.8 shows the simulation results for the uni-axial (x, y and z) and isostatic yield testing for different numbers of revolution. Unexpectedly the strength for 0.5 revolutions is the lowest. The maximum strengths result for one total revolution per fibre length. For 0.25 and 0.75 revolution the strengths are comparably equal and do not differ significantly. What might cause this unexpected behaviour is the different elastic strain depending on the twisting. Subsequently the

equivalent elastic strain is determined to proof this presumption. The equation for the strain tensor (Equation (2.10)) is mentioned in section 2.2.3.1 as well as the basics of the equivalent elastic strain determination. The equivalent elastic strain ϵ_{el} is obtained from the unloading step. After the compaction step the RVE is unloaded to a final stress and the equivalent elastic unloading strain is determined. Detailed explanation can be found in Loidolt et al. [17].

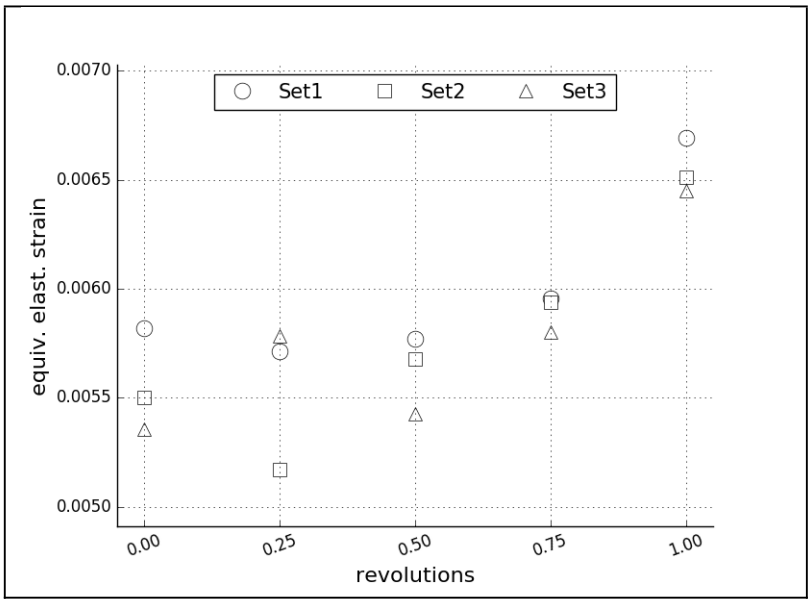

Figure 3.9: Equivalent elastic strain of the packing at the relieve step after compression for three different RVE sets per revolution.

In Figure 3.9 the equivalent elastic strains are depicted versus the particle revolution. A trend for higher elastic strains with higher revolution can be determined. However the equivalent elastic strain is slightly diverging for a single number of revolution, especially noticeable for 0.25. Additionally it needs to be mentioned that a variation of the equivalent elastic strain of about 0.0005 of different sets is not significant compared to the occurring variations of resulting yield strengths. The termination of the yield step and strength is reached when the plastic deformation ϵ_{pl} reaches 0.002, Equation (2.11). The equivalent elastic strain (Figure 3.9) with an arithmetic mean of 0.0058, is in comparison to the yield termination condition two to three times bigger. The assumption for this yielding criterion in Loidolt et al. [17] is that the elastic strain is small compared to the plastic deformation. However with the simulation of non-spherical particles controversial behaviour is observed. Further adaptation of the termination yield criterion might be necessary.

The equivalent elastic strain during unloading influences the contact area. High equivalent elastic strain results in a loss of contact area after the compaction step. A correlation between the yield strengths and equivalent elastic strain can be noticed, Figure 3.8 and

Figure 3.9 respectively. However a direct connection between the equivalent elastic strain during unloading and the yield strengths can not be found.
For 1.0 revolution per particle length the strength and equivalent elastic strain show the highest values although an increasing equivalent elastic strain leads to a loss of contact area. Therefore additionally to the elastic equivalent strain the compaction pressure needs to be factored in. More twist may result in higher compaction pressure, subsequently more contact area and higher strengths occur. Additionally the equivalent elastic strain increases. The increasing pressure is a consequence of the twisting of the particles and the following stronger deformation of the particles to fulfil the compaction termination criterion of 0.85 relative packing density. Thus the equivalent pressure stress p (in detail explained in Loidolt et al. [17]) at the end of the compaction step is examined. The equivalent pressure represents the arithmetic mean of the principal normal stresses of the stress tensor. The analysis of the equivalent pressure stress is depicted in Figure 3.10.

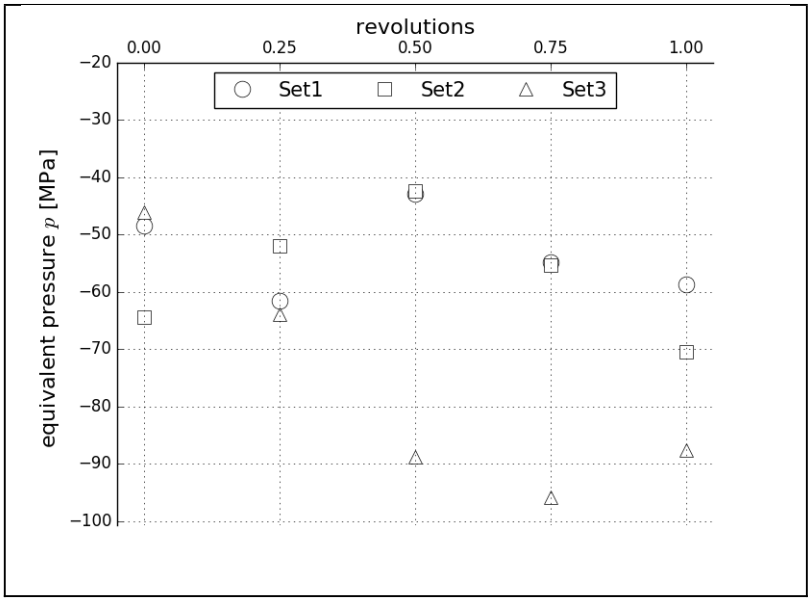

Figure 3.10: The equivalent pressure after the compaction to 0.85 relative density depending on the particles revolution for three different initial sets per particle revolution.

Comparing the three Figures (Figure 3.9, Figure 3.8 and 3.10) emphasises the understanding of the relation between equivalent elastic strain, equivalent pressure and strength. Figure 3.9 and 3.10 depict the equivalent pressure and equivalent elastic strain of the same set (Set 1 to Set 3) per particle revolution. High equivalent pressures after compaction may lead to higher equivalent elastic strains, most notably for one revolution. However this correlation is not valid for other revolutions. For 0.5 revolution and Set 3 the equivalent pressure after compaction exceeds Set 1 and Set 2, but the equivalent

elastic strain during unloading is lower than for the other two sets with the same revolution. Although there are correlations between equivalent pressure after compaction, the equivalent elastic strain during unloading, the yield strength, and the number of revolution further studies with different lengths and different particle shapes are reasonable to may find direct correlations and to deepen the knowledge and understanding of the uniaxial compression and yield strength behaviour. Additionally more sets are necessary to diminish effects of individual set configurations on the results.

Chapter 4

Conclusion & Outlook

Non-spherical particles are implemented in the MPFEM simulation environment developed by Loidolt et al. [17]. The goal of this MPFEM model is to simulate the behaviour of powder compacts and to examine the resulting yield behaviour. To achieve this goal two different simulation procedures are followed. First, an RVE with randomly distributed particles is generated in *LIGGGHTS ®*. Second, the generated RVE is transferred into the *Abaqus CAE - Simulia™* environment where the compaction of the RVE is simulated and the yield strengths are determined.

Convergence studies investigate the influence of the simulation parameters on the resulting strengths. First the mesh fineness is varied. From an element number of four elements per particle diameter onwards converging behaviour is observed. The particle number inside an RVE is the second investigated simulation parameter. A convergence behaviour for the tension strength of RVEs with 150 particles onwards can be identified. For the compression and isostatic yield tests the strengths do not show converging behaviour. Different initial packing configurations for the same particle number lead to varying strengths. The RSD is relatively small for a number of 100 particles in the RVE. Simulation time and costs emphasise the decision for further simulations of RVEs with 100 particles. For all examined solver time step sizes an approximately constant strength is obtained. To guarantee stable simulations for different particle shapes a solver time step size of 10^{-4}s is chosen. The mass scale factor negatively influences the simulation result if too high mass factors are applied and the resulting strengths are altered due to inertia effects. From a mass scale factor lower than 10^5 onwards about constant strengths are obtained. A mass scale factor of 10^4 is chosen. The RVE with the simulation parameters from the convergence studies are undertaken further studies concerning the effects of the geometrical particle properties on the strengths. The revolution of the particle per particle length is varied, whereas all other particle properties are kept constant. Complex strength behaviour is determined. The mechanistic model allows for understanding the correlation between the equivalent pressure after compaction, the equivalent elastic strain during unloading and the yield strengths. The idea of direct

correlation between higher strengths with increasing twist of the particles can not be followed. The lowest strengths are obtained for 0.5 revolution of the particles, whereas the highest strength is obtained for one revolution per particle length.

This work constitutes the opportunity to mechanistically understand the influences of different properties on the resulting strengths. Nevertheless, numerous improvements need to be done. To guarantee equal initial RVEs, either an appropriate termination criterion for the packing generation in *LIGGGHTS®* needs to be realized or the total RVE generation is implemented into the *Abaqus CAE - Simulia™* environment. Further improvements include the iterative procedure to determine the process parameters with convergence studies. In general more simulations are necessary. Not only in terms of higher number of different initial packings for one specific parameter set but also additional particle shapes and poly-disperse powders should be investigated. These further improvements may lead to diminish fluctuations of the strengths and may lead to a better understanding of the influences of geometrical shapes on the resulting strengths. If future studies further indicate the imbalance of plastic strain and equivalent elastic strain an appropriate yield criteria needs to be developed for non-spherical particles. Besides the already mentioned improvements in terms of simulation environment, the results should be compared with experimental results.

Bibliography

[1] Nouha Abdelmoula et al. "A study on the uniqueness of the plastic flow direction for granular assemblies of ductile particles using discrete finite-element simulations". In: *Journal of the Mechanics and Physics of Solids* 109 (2017), pp. 142–159. DOI: 10.1016/j.jmps.2017.07.021.

[2] W.J. Chung, J.W. Cho, and T. Belytschko. "On the dynamic effects of explicit FEM in sheet metal forming analysis". In: *Engineering Computations* 15.6 (1998), pp. 750–776. DOI: 10.1108/02644409810231880.

[3] Stephen Edge et al. "The mechanical properties of compacts of microcrystalline cellulose and silicified microcrystalline cellulose". In: *International Journal of Pharmaceutics* 200 (2000), pp. 67–72. DOI: 10.1016/S0378-5173(00)00343-4.

[4] S J Eichhorn and R J Young. "The Young's modulus of a microcrystalline cellulose". In: *Cellulose* 8.3 (2001), pp. 197–207. URL: http://dx.doi.org/10.1023/a:1013181804540.

[5] P. Evesque. "Fluctuations, correlation and representative elementary volume (REV) in granular materials". In: *Poudres & Grains* 11 (June 2000), pp. 6–17. arXiv: 0506385 [cond-mat]. URL: http://arxiv.org/abs/cond-mat/0506385.

[6] Roger Gaudreault, Theo G.M. Van De Ven, and M. A. Whitehead. "Mechanisms of flocculation with poly(ethylene oxide) and novel cofactors". In: *Colloids and Surfaces A: Physicochemical and Engineering Aspects* 268.1-3 (2005), pp. 131–146. DOI: 10.1016/j.colsurfa.2005.04.044.

[7] I. M. Gitman, H. Askes, and L. J. Sluys. "Representative volume: Existence and size determination". In: *Engineering Fracture Mechanics* 74.16 (2007), pp. 2518–2534. DOI: 10.1016/j.engfracmech.2006.12.021.

[8] Gustaf Gustafsson, Hans Åke Häggblad, and Pär Jonsén. "Multi-particle finite element modelling of the compression of iron ore pellets with statistically distributed geometric and material data". In: *Powder Technology* 239 (2013), pp. 231–238. ISSN: 00325910. DOI: 10.1016/j.powtec.2013.02.005.

[9] Bruno C. Hancock, Sophie Dorothee Clas, and Karen Christensen. "Micro-scale measurement of the mechanical properties of compressed pharmaceutical powders. 1: The elasticity and fracture behavior of microcrystalline cellulose". In: *International Journal of Pharmaceutics* 209.1-2 (2000), pp. 27–35. DOI: 10.1016/S0378-5173(00)00541-X.

[10] Barthélémy Harthong, Didier Imbault, and Pierre Dorémus. "The study of relations between loading history and yield surfaces in powder materials using discrete finite element simulations". In: *Journal of the Mechanics and Physics of Solids* 60.4 (2012), pp. 784–801. DOI: 10.1016/j.jmps.2011.11.009.

[11] Z. Hashin. "Analysis of Composite Materials—A Survey". In: *Journal of Applied Mechanics* (1983), pp. 481–505. DOI: 10.1115/1.3167081.

[12] Takehiko Horio, Masatoshi Yasuda, and Shuji Matsusaka. "Effect of particle shape on powder flowability of microcrystalline cellulose as determined using the vibration shear tube method". In: *International Journal of Pharmaceutics* 473.1-2 (2014), pp. 572–578. DOI: 10.1016/j.ijpharm.2014.07.040.

[13] Fen Huang et al. "Multi-particle FEM simulation of 2D compaction on binary Al/SiC composite powders". In: *Powder Technology* 314 (2017), pp. 39–48. DOI: 10.1016/j.powtec.2017.03.017.

[14] Roman Huber. "Modellierung und Vernetzung von Laktose- und Zellulosepartikeln für die Multiple-Partikel-Finite-Elemente-Methode". Bachelor's Thesis. Graz University of Technology: Institute of Process and Particle Engineering, 2017.

[15] J. F. Jerier et al. "Study of cold powder compaction by using the discrete element method". In: *Powder Technology* 208.2 (2011), pp. 537–541. DOI: 10.1016/j.powtec.2010.08.056.

[16] Christoph Kloss et al. "Models, algorithms and validation for opensource DEM and CFD-DEM". In: *Progress in Computational Fluid Dynamics, An International Journal* 12.2/3 (2012), p. 140. DOI: 10.1504/PCFD.2012.047457.

[17] Peter Loidolt, Manfred H. Ulz, and Johannes Khinast. "Modeling Yield Properties of Compacted Powder using a Multi-Particle Finite Element Model with Cohesive Contacts". In: *Powder Technology* (under review: 2018).

[18] Fernando J. Muzzio, Troy Shinbrot, and Benjamin J. Glasser. "Powder technology in the pharmaceutical industry: The need to catch up fast". In: *Powder Technology* 124.1-2 (2002), pp. 1–7. DOI: 10.1016/S0032-5910(01)00482-X.

[19] Ann Sofie Persson and Göran Frenning. "An experimental evaluation of discrete element simulations of confined powder compression using an extended truncated-sphere model". In: *Powder Technology* 284 (2015), pp. 257–264. DOI: 10.1016/j.powtec.2015.06.053.

[20] Gottfried Segner. "Generieren dichter Packungen von verschieden förmigen Partikeln mit der DEM-Methode". Bachelor's Thesis. Graz University of Technology: Institute of Process and Particle Engineering, 2017.

[21] Dassault systemes Simulia. *Abaqus Documentation, Version 6.13*. URL: http://dsk.ippt.pan.pl/docs/abaqus/v6.13/index.html (visited on 04/17/2018).

[22] I. C. Sinka et al. "The effect of processing parameters on pharmaceutical tablet properties". In: *Powder Technology* 189.2 (2009), pp. 276–284. DOI: 10.1016/j.powtec.2008.04.020.

[23] M. Stroeven, H. Askes, and L. J. Sluys. "Numerical determination of representative volumes for granular materials". In: *Computer Methods in Applied Mechanics and Engineering* 193.30-32 (2004), pp. 3221–3238. DOI: 10.1016/j.cma.2003.09.023.

[24] Changquan Calvin Sun. "Mechanism of moisture induced variations in true density and compaction properties of microcrystalline cellulose". In: *International Journal of Pharmaceutics* 346.1-2 (2008), pp. 93–101. DOI: 10.1016/j.ijpharm.2007.06.017.

[25] Wei-Jhe Sun, Sanjeev Kothari, and Changquan Calvin Sun. "The relationship among tensile strength, Young's modulus, and indentation hardness of pharmaceutical compacts". In: *Powder Technology* 331 (2018). DOI: 10.1016/j.powtec.2018.02.051. URL: http://linkinghub.elsevier.com/retrieve/pii/S0032591018301785.

[26] C. Y. Wu et al. "Modelling the mechanical behaviour of pharmaceutical powders during compaction". In: *Powder Technology* 152.1-3 (2005), pp. 107–117. DOI: 10.1016/j.powtec.2005.01.010.

[27] Jonathan P.K. Seville; Chuan-Yu Wu. *Particle technology and engineering : an engineer's guide to particles and powders : fundamentals and computational approaches*. Butterworth Heinemann, 2016. ISBN: 0-08-098337-5, 978-0-08-098337-0.

[28] Jing Zhang. "A study of compaction of composite particles by multi-particle finite element method". In: *Composites Science and Technology* 69.13 (2009), pp. 2048–2053. DOI: 10.1016/j.compscitech.2008.11.020.

[29] Y. X. Zhang, X. Z. An, and Y. L. Zhang. "Multi-particle FEM modeling on microscopic behavior of 2D particle compaction". In: *Applied Physics A: Materials Science and Processing* 118.3 (2014), pp. 1015–1021. DOI: 10.1007/s00339-014-8861-x.

[30] Haibo Zhao et al. "Studying cellulose fiber structure by SEM, XRD, NMR and acid hydrolysis". In: *Carbohydrate Polymers* 68.2 (2007), pp. 235–241. DOI: 10.1016/j.carbpol.2006.12.013.

List of Figures

List of Tables

Abbreviations & Nomenclature

Abbreviations	
DEM	Discrete Element Method
FEM	Finite Element Method
MPFEM	Multiparticle Finite Element Method
RSD	Relative Standard Deviation
RVE	Representative Volume Element

Greek Symbols	
δ_N	normal displacement
$\dot{\delta_N}$	normal relative velocity
δ_T	tangential displacement
$\dot{\delta_T}$	tangential relative velocity
δ_0	cohesion interaction length
ϵ	coefficient of restitution
$\boldsymbol{\epsilon}$	strain tensor
$\boldsymbol{\epsilon_{el}}$	elastic strain tensor
ϵ_{pl}	equivalent plastic strain
$\epsilon_{plastic}$	plastic strain
$\boldsymbol{\epsilon_{yp}}$	strain tensor at the yield point
μ	frictional coefficient
ν	Poisson ratio
ρ	density
$\boldsymbol{\sigma}$	stress tensor
$\sigma_{coh_{max}}$	cohesion stress maximum

Latin Symbols	
$a_{box_{deformation}}$	box deformation acceleration
a_{Sphere}	sphere acceleration
d	damping factor
E	Youngs Modulus
F	force
F_{max}	maximal force, occurring on box edges
$fac_{scale\ mass}$	mass scale factor
$frac_{add,layer}$	additional-layer-fraction parameter
k	normal stiffness
$l_{element}$	element size
l_e	final length of box
l_0	initial length of box
$l_{particle\ to\ center}$	distance particle to box center
p	equivalent pressure stress
r	particle radius
t_{sim}	total simulation time
Δt	time step in *LIGGGHTS®*
Δt_{solver}	solver time step size in *Abaqus CAE - Simulia™*
v	initial particle velocity
Δv	standard deviation of the velocity
Δx_{add}	thickness of additional layer
Δx_{box}	incremental box deformation